Thermal Switching Error versus Delay Tradeoffs in Clocked QCA Circuits

Sanjukta Bhanja , *Member, IEEE* Sudeep Sarkar , *Senior Member, IEEE*

***Abstract*— The Quantum-dot Cellular Automata (QCA) model offers a novel nano-domain computing architecture by mapping the intended logic onto the lowest energy configuration of a collection of QCA cells, each with two possible ground states. A four phased clocking scheme has been suggested to keep the computations at the ground state throughout the circuit. This clocking scheme, however, induces latency or delay in the transmission of information from input to output. In this paper we study the interplay of computing error behavior with delay or latency of computation induced by the clocking scheme. Computing errors in QCA circuits can arise due to the failure of the clocking scheme to switch portions of the circuit to the ground state with change in input. Some of these non-ground states will result in output errors and some will not. Larger the size of each clocking zone, i.e. greater the number of cells in each zone, the more is the probability of computing errors. However, larger clocking zones implies faster propagation of information from input to output, i.e. reduced delay. Current QCA simulators compute just the ground state configuration of a QCA arrangement. In this paper, we offer an efficient method to compute the N-lowest energy modes of a clocked QCA circuit. We model the QCA cell arrangement in each zone using a graph-based probabilistic model, which is then transformed into a Markov tree structure defined over subsets of QCA cells. This tree structure allows us to compute the N-lowest energy configurations in an efficient manner by local message passing. We analyze the complexity of the model and show it to be polynomial in terms of the number of cells, assuming a finite neighborhood of influence for each QCA cell, which is usually the case. The overall low-energy spectrum of multiple clocking zones is constructed by concatenating the low-energy spectra of the individual clocking zones. We demonstrate how the model can be used to study the trade-off between switching errors and clocking zones.**

I. Introduction

The anticipated scaling problem with CMOS has lead to a fresh reconsideration of alternative emerging technologies. Opinions differ as to which emerging technology will succeed CMOS. One nanodevice that has potential for radically different forms of computing is the Quantum-dot cellular automata (Electronic, Magnetic and Molecular-QCA) [1], [2], [3], [4], where nano-effects, such as device to device coupling, which can be a problem in nano-electronics, is exploited for computing. Each cell consists of one or more electrons that can exist in two or more dots, with two ground state configurations. These two ground states can be taken to represent the logic states of zero and one. Two or more cells interact by Coulombic interactions, with an arrangement of cells settling to the lowest energy state. Traditional logic circuits can be built by mapping the logic onto the ground state configuration [5], [6]. Initial criticisms about the difficulty of converging to the ground state has been addressed by using the concept of four phased adiabatic clocking. The goal of the phased clocking mechanism is to "pump" the logic information from the inputs to the output. The adiabatic aspect of the clocking seeks to keep the circuit at ground state. Since there is no flow of electrons involved, there is no need for interconnects, and it has potential for extremely low-power computing, even below the traditional kT [7], [8].

Experimental demonstration of QCA technology has occurred at a steady pace. Both individual QCA cells (semiconductor and metallic) and multiple QCA arrangements (wires, clocked wires, majority logic, AND, OR, shift registers, memory) have been fabricated and tested [9], [10], [11], [12], [13], [14]. It is interesting to note that the range of devices experimentally demonstrated is similar to that for the more popular CNT-FET based ones: inverter, NOR, memory cell, AC ring oscillator [15], [16]. Significant progress is also being made in using molecules and magnets to implement QCAs [4], [3], which will make it possible to operate at room temperature, possibly alleviating the initial criticisms of this technology.

QCA computations can be abstracted by Coulombic interactions between cells, each of which contain quantum entangled electrons. There are many variations of the design of the basic cell structure. The common theme among all these designs is that the ground state of each cell can be achieved by 2 different configurations, which can be used to represent two logic states, 0 or 1. Logical computation is specified by the ground, i.e. minimum energy, state of the circuit. To drive a circuit towards this ground state with every change in input, clocked QCA circuit designs have been proposed. The overall circuit is divided into zones, with each zone driven by one of the four clocks. As an example, consider a QCA wire shown in Fig. 1 with 2 cells per zone. The clocks are phase shifted versions of each other. The task of the clock is to repeatedly depolarize (nullify the state) a cell and latch the state to zero or one, and hold the new state, based on the states of the surrounding cells. A depolarized cell state does not effect the surrounding cells. The clock phases of two consecutive zones are staggered so that the cells in one zone can "drive" the cells in the other zone. In effect, the four phased clocking scheme helps pump the information from the input to the output, delaying the transmission of information from the input to the output. This delay is proportional to the number of clock zones. In passing, we may also note that another benefit of the clock is in acting as a power source, however, we are not concerned with that aspect in this paper.

There are four kinds of errors in QCA operations: decay errors, dynamic errors, background charge fluctuations, and switching (or thermal) errors. They were analyzed and experimentally quantified for metal-dot QCA in [14] and expected to be also present for molecular QCAs. Decay error occurs due to the failure of retaining the state of a cell, however, the time constants of such effects is larger than the GHz operating point of QCA clocks. Dynamic errors can occur when the clock frequencies approach the time constants for tunneling events. This would be a problem only for ultra high frequencies ($\gg$ GHz). Random background charge drifts in the order of minutes could

Sanjukta Bhanja is with the Department of Electrical Engineering University of South Florida, Tampa, FL-33620. USA
Email: bhanja@eng.usf.edu

Sudeep Sarkar is with the Deptartment of Computer Science and Enginering University of South Florida,Tampa, FL-33620
Email: sarkar@cse.usf.edu

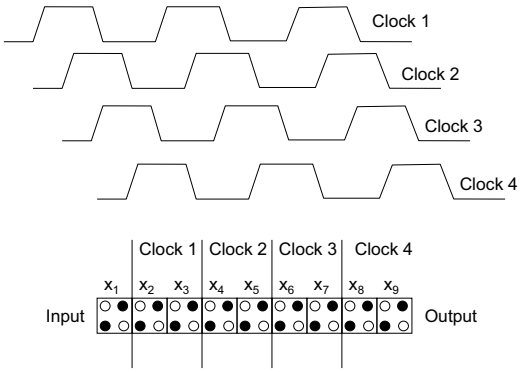

Fig. 1. Example of a clocked wire segment.

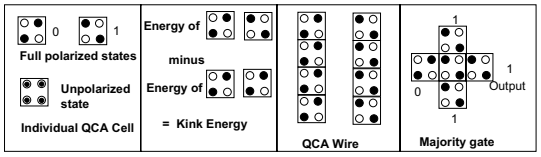

Fig. 2. QCA basics and the traditional use of QCAs for logic computing. Each cell exists in a combination of two polarized states. The kink energy between two cells is defined to be the difference between the energy if the cells have opposite states and the energy if the cells have same states. A linear arrangement of cells has two ground state configurations and can act as a wire. Majority logic is natural to QCA and is the basic gate for QCA circuits.

be a problem, but there is possibility that new fabrication methods can control it. By far, the most dominant form of errors in QCA devices are expected to be switching or thermal errors. Within each clocking zone it is necessary that the cell stay in the ground state. This is achieved by using adiabatic clocking so that states are not changed suddenly. However in practice, imperfect adiabatic clocking and increased temperatures can result in error conditions when the cells in a zone settle down to excited states. At temperature T, the probability for these kinds of thermally induced errors is given by [14]

$$p_{th} \propto \exp(-\Delta/kT) \tag{1}$$

where k is the Boltzman constant and Δ is the energy gap between the ground state and the next excited state. Thus, to analyze these switching errors in QCA circuits, we need to be able reason about near ground states in each clocking zone. However, current QCA simulators cannot compute such states.

Simulators such as QBert [17], Fountain-Excel simulation, nonlinear simulation [18], [19], and digital simulation [19] can estimate the ground state of the cells. There are also quantum mechanical simulators such as AQUINAS [20] and the Coherence vector simulation engine in the QCADesigner [19], both of which perform iterative quantum mechanical simulation by factorizing the joint wave function over all cells into a product of individual cell wave functions (Hartree-Fock approximation). They result in accurate estimates of ground states, cell polarization (or probability of cell state), temporal progress, and thermal effects, however, only for the ground state. The only work that computes the non-ground state is [21], but it computes just one lowest energy state configuration that causes output errors. It cannot find all the near ground states and it does not provide a clock zone by clock zone energy spectrum. *To fully study the error behavior of designs it also important to consider excited states that can arise in each clocking zone. Of particular interest are the low-energy circuit states that are near the ground state.*

The inference of low-energy non-ground states requires an exploration of the QCA cell state configuration space, whose size is exponential in the number of cells in each clocking zone. The only currently available approach, that we are aware of, to accomplish this is using simulated annealing search [22]. Simulated annealing search is a stochastic search technique whose probability of success depends on the number of iterations and how slowly the system is driven towards the convergence point. For a circuit with 6 cells, it can take 10,000's of iterations. In this paper, we present a method based on maximum likelihood probabilistic inference to infer N-lowest energy configurations. The inference is conducted with a graphical probabilistic model that is built to represent the joint probability of the state configuration.

Starting from a quantum mechanical Hamiltonian, we show that the quantum mechanical spectrum can be expressed as a perturbation of the semi-classical spectrum for range of dot-to-dot tunneling energies envisioned for QCAs. We compute the semi-classical spectrum using graphical probabilistic models, specifically Markov networks [23], [24]. In these graphical representations, the nodes denote the random quantities of interest, which are the states of the individual QCA cell, and links denote direct dependencies. The structure of the network is dictated by the layout of the devices and are quantified by probabilities determined by Gibbs energy. This exactly models the joint probability of the cell states, based on the Boltzman distribution. For efficient and *exact* inference, we first convert this Markov network into a tree-structured Markov network, called the junction tree, defined over subset (cliques) of nodes. Maximum likelihood inference of the cell states then just involves local message passing between the nodes in this junction tree. The N-most likely states correspond to the N-lowest energy states. Markov models are commonly used in reliability studies of circuits [25], [26], [27], where average case behavior is computed. We take this idea farther by (i) exploring non-ground states, (ii) strongly coupling device physics into the model, (iii) and using an accurate probabilistic computing model.

In the next section, we present the Markov model of QCA computations and how it can be constructed. In Section III, we present the probability updating schemes that allows us to reason about the low-energy configurations in one clock zone, which is used to construct the energy spectrum of multiple zones in Section IV. We validate and present results on commonly used QCA circuit elements in Section VI. We discuss complexity issues in Section VII and conclude with Section VIII.

II. Markov Model of QCA Computation

The basic unit of computation is a cell consisting of two electrons that can exist in four possible quantum dots. There are two possible ground state (minimum energy) configurations for

each cell, corresponding to the two possible diagonal occupancies (see Fig. 2). These two states are used to represent the logic states 0 and 1. While there is quantum tunneling between dots in the same cell, there is no quantum tunneling between neighboring cells. However, neighboring cells effect each other by modifying the potential energies through Coulombic interactions, which in turn effect the ground state configuration of a cell arrangement.

Current effort in QCA has been to build logic circuits by mapping the logic onto the ground state configuration. Given that the total energy is composed out of the pairwise Coulombic interactions between cells, the ground state configuration can be described as minimizing the total kink energy. The kink energy between two cells is defined to be the difference in energy if the cells have opposite states (or polarizations) and the energy if the cells have same states (or polarizations). Thus, a linear arrangement of cells has two ground state configurations, without any kinks, and can act as a wire (see Fig. 2). Another basic logic element is the 3-input majority gate that can be constructed by arranging the cells as shown in Fig. 2. To keep the QCA circuit at ground state, an adiabatic four phased clocking scheme has been proposed that modulates the tunneling energies between the dots in a cell. The clocking scheme controls the flow of information in a QCA circuit by driving each cell through depolarized state, latching phase, and hold phase, and then back to a depolarized state. The adiabatic aspect of the clock keeps the circuit at ground state. Note that computation errors can arise if the circuit goes out of ground state. Of particular interest are states that are close to the ground states.

Finding the exact excited spectrum of a general quantum mechanical system is an open research area. While there is lot of research on computing the ground state of quantum systems, there is few works in computing the excited states [28]. Most methods resort to approximate methods by approximating the Hamiltonian using for example Hartree-Fock or density functional methods or quantum Monte Carlo. In the QCA case, since there is no quantum tunneling between neighboring cells and the tunneling energy between the dots in a cell are in general low, some recent studies [29], [30] have used the semi-classical Boltzman distribution as a model. This model suffices. In this paper, we show using *ab initio* calculations that the quantum-model based distribution is indeed close to the semi-classical Boltzman model and that the former can be approximated as a perturbed version of the latter for practical QCA circuits.

A. The Quantum Model

Since there is no quantum interaction between cells, the overall state vector of a collection of N QCA cells, which is referred to as the wave-function and denoted by $|\Psi\rangle$, can be expressed as the tensor product of the individual cell states. We denote the two possible, orthogonal, states of the i-th QCA cell by $\Psi_i = |1\rangle$ and $\Psi_i = |0\rangle$. Then, the multiple cell basis states are given by the tensor product

$$|\Psi\rangle = |\Psi_1\rangle \otimes |\Psi_2\rangle \otimes \cdots |\Psi_N\rangle \tag{2}$$

The evolution of the wave function is determined by the underlying Hamiltonian $\mathbf{H}$, which, in the absence of quantum interactions, is given by the sum of the Hamiltonians of the individual QCA cells.

$$\begin{aligned} \mathbf{H} &= \mathbf{1}\otimes\cdots\mathbf{1}\otimes\mathbf{H}_1 + \mathbf{1}\otimes\cdots\mathbf{1}\otimes\mathbf{H}_2\otimes\mathbf{1} + \cdots + \mathbf{H}_N\otimes\mathbf{1}\otimes\cdots\mathbf{1} && (3)\\ &= \mathcal{H}_1 + \mathcal{H}_2 + \cdots + \mathcal{H}_N && (4)\end{aligned}$$

where $\mathbf{1}$ is the unit element (2 by 2 identity matrix) and $\mathbf{H}_i$'s are the individual Hamiltonian, 2 by 2, matrices that have been shown to be adequately approximated by the Hartree approximation [31].

$$\mathbf{H}_i = \begin{bmatrix} -\frac{1}{2}\sum_j E_{ij}^{(k)} P_j & -\gamma \\ -\gamma & \frac{1}{2}\sum_j E_{ij}^{(k)} P_j \end{bmatrix} = \begin{bmatrix} -E_i & -\gamma \\ -\gamma & E_i \end{bmatrix} \tag{5}$$

where $E_{ij}^{(k)}$ is the electrostatic kink energy between the i-th and j-th cells, representing the energy cost of the cells with full, but opposite polarizations.

The expected value of any observable, $\langle\hat{A}\rangle$, can be expressed in terms of the wave function as $\langle\hat{A}\rangle = \langle\Psi|\hat{A}|\Psi\rangle$ or equivalently as $\mathrm{Tr}[\hat{A}|\Psi\rangle\langle\Psi|]$, where Tr denotes the trace operation, $\mathrm{Tr}[\cdots] = \langle 1|\cdots|1\rangle + \langle 0|\cdots|0\rangle$. The term $|\Psi\rangle\langle\Psi|$ is known as the density operator, $\hat{\rho}$. Expected value of any observable of a quantum system can be computed if $\hat{\rho}$ is known.

When the QCA cell array is in thermodynamic equilibrium with a stationary heat bath, the steady state (thermal) density matrix is given by [32]:

$$\rho_{th} = \frac{e^{-\beta\mathbf{H}}}{\mathrm{Tr}(e^{-\beta\mathbf{H}})} \tag{6}$$

where $\beta = \frac{1}{kT}$, with k being the Boltzman constant, T the temperature, and Tr is the trace operation. The denominator, $Z = \mathrm{Tr}(e^{-\beta\mathbf{H}})$, is the quantum mechanical counterpart of the canonical partition function. Using the expansion of the global Hamiltonian in terms of the local ones (Eq. 4), we have

$$\rho_{th} = \frac{1}{Z} e^{-\sum_k \beta\mathcal{H}_k} \tag{7}$$

The individual Hamiltonians, $\mathbf{H}_i$, can be expressed in terms of their eigenvalues (energy levels), Ω_{-1} and Ω_{+1}, and eigenvectors $(a_{-1}, b_{-1})^T$ and $(a_{+1}, b_{+1})^T$.

$$\mathbf{H}_i = \Omega_{-1}\begin{bmatrix} a_{-1}^2 & a_{-1}b_{-1} \\ a_{-1}b_{-1} & b_{-1}^2 \end{bmatrix} + \Omega_{+1}\begin{bmatrix} a_{+1}^2 & a_{+1}b_{+1} \\ a_{+1}b_{+1} & b_{+1}^2 \end{bmatrix} \tag{8}$$

where $\Omega_{-1} = -\sqrt{E_i^2+\gamma^2}$, $\Omega_{+1} = \sqrt{E_i^2+\gamma^2}$, $a_{-1}^2 = \frac{1}{2}\frac{\sqrt{E_i^2+\gamma^2}+E_i}{\sqrt{E_i^2+\gamma^2}}$, $a_{+1}^2 = \frac{1}{2}\frac{\sqrt{E_i^2+\gamma^2}-E_i}{\sqrt{E_i^2+\gamma^2}}$, $b_{-1}^2 = \frac{1}{2}\frac{\sqrt{E_i^2+\gamma^2}-E_i}{\sqrt{E_i^2+\gamma^2}}$, an $b_{+1}^2 = \frac{1}{2}\frac{\sqrt{E_i^2+\gamma^2}+E_i}{\sqrt{E_i^2+\gamma^2}}$, For notational ease we will use

$$\mathbf{H}_i = \Omega_{-1}\rho_{-1} + \Omega_{+1}\rho_{+1} = \sum_{y_i=\{-1,+1\}} \Omega_{y_i}\rho_{y_i} \tag{9}$$

The diagonal entries of the ρ matrices represent the probabilities of the corresponding states. We will refer to them as $\Omega_{y_i}(-1)$

and $\Omega_{y_i}(+1)$. For instance, $\Omega_{y_{-1}}(-1) = a_{-1}^2$ and $\Omega_{y_{-1}}(+1) = b_{-1}^2$. Using this we can show that

$$\mathcal{H}_i = \sum_{y_i=\{-1,+1\}} \Omega_{y_i} (\mathbf{1} \otimes \mathbf{1} \otimes \cdots \rho_{y_i} \cdots \otimes \mathbf{1}) \tag{10}$$

Using this in Eq. 7 we have

$$\begin{aligned}
\rho_{th} &= \frac{1}{Z} \prod_i \sum_{y_i=\{-1,+1\}} e^{-\beta \Omega_{y_i}} (\mathbf{1} \otimes \mathbf{1} \otimes \cdots \rho_{y_i} \cdots \otimes \mathbf{1}) && (11)\\
&= \frac{1}{Z} \sum_{y_1,\cdots,y_N} e^{-\beta \sum_i \Omega_{y_i}} \prod_i (\mathbf{1} \otimes \mathbf{1} \otimes \cdots \rho_{y_i} \cdots \otimes \mathbf{1}) && (12)\\
&= \frac{1}{Z} \sum_{y_1,\cdots,y_N} e^{-\beta \sum_i \Omega_{y_i}} (\rho_{y_1} \otimes \cdots \otimes \rho_{y_i} \otimes \cdots \otimes \rho_{y_N}) && (13)
\end{aligned}$$

Given that each cell has 2 states, ρ_{th} is a $2^N \times 2^N$ matrix with the diagonal entries representing the probability of the different possible combination of the states. Let $\{x_1, \cdots, x_N\}$ represent a state combination of the cells, then

$$P_\rho(x_1, \cdots, x_N) = \frac{1}{Z} \sum_{y_1,\cdots,y_N} e^{-\beta \sum_i \Omega_{y_i}} (\rho_{y_1}(x_1) \otimes \cdots \otimes \rho_{y_i}(x_i) \otimes \cdots \otimes \rho_{y_N}(x_N)) \tag{14}$$

where we have used the shortened notation $\rho_{y_i}(x_i)$ with $x_i = \{-1, 1\}$, to refer to the diagonal entries of ρ_{y_i}, which are the probabilities of these two states for the eigenstate if the i-the cell. The partition function can be shown to be

$$\begin{aligned}
Z &= \mathrm{Tr} \sum_{y_1,\cdots,y_N} e^{-\beta \sum_i \Omega_{y_i}} (\rho_{y_1} \otimes \cdots \otimes \rho_{y_N}) && (15)\\
&= \sum_{x_1,\cdots,x_N} \sum_{y_1,\cdots,y_N} e^{-\beta \sum_i \Omega_{y_i}} (\rho_{y_1}(x_1) \otimes \cdots \otimes \rho_{y_N}(x_N)) && (16)\\
&= \sum_{y_1,\cdots,y_N} e^{-\beta \sum_i \Omega_{y_i}} \sum_{x_1,\cdots,x_N} (\rho_{y_1}(x_1) \otimes \cdots \otimes \rho_{y_N}(x_N)) && (17)\\
&= \sum_{y_1,\cdots,y_N} e^{-\beta \sum_i \Omega_{y_i}} && (18)
\end{aligned}$$

Thus the complete quantum distribution function is given by

$$P_\rho(x_1, \cdots, x_N) = \frac{1}{\sum_{y_1,\cdots,y_N} e^{-\beta \sum_i \Omega_{y_i}}} \sum_{y_1,\cdots,y_N} e^{-\beta \sum_i \Omega_{y_i}} (\rho_{y_1}(x_1) \otimes \cdots \otimes \rho_{y_N}(x_N)) \tag{19}$$

B. Semi-classical Approximation

In practice solving Eq. 19 is computationally expensive, so we resort to approximations. One such approximation uses the fact that the tunneling energy γ will be very low compared to the kink energies. It is envisioned that $\frac{\gamma}{E^{(k)}}$ would be in the order of 10^{-3} or less [30]. Thus, this means that one of the diagonal values of ρ_{y_i} will be close to 1, while the other will be close to 0. In order words, the cell polarizations will be close to -1 or 1. Let $\rho_{-1}(-1) = 1-\varepsilon$ and $\rho_{-1}(+1) = \varepsilon$, and correspondingly $\rho_{+1}(-1) = \varepsilon$ and $\rho_{+1}(+1) = 1-\varepsilon$, with ε being in the order of 10^{-6} for $\frac{\gamma}{E^{(k)}}$ in the order of 10^{-3}. Using this approximation, the tensor products in Eq. 19 will be product of various powers of ε and $1-\varepsilon$. Ingoring higher order terms of ε, we can show that

$$\begin{aligned}
P_\rho(x_1, \cdots, x_N) &\approx \frac{1}{\sum_{y_1,\cdots,y_N} e^{-\beta \sum_i \Omega_{y_i}}} \left[e^{-\beta \sum_i \Omega_{x_i}} (1-\varepsilon)^N + \varepsilon (1-\varepsilon)^{N-1} \sum_{y_i \neq x_i} e^{-\beta \sum_i \Omega_{y_i}} \right] && (20)\\
&\approx \frac{1}{\sum_{y_1,\cdots,y_N} e^{-\beta \sum_i \Omega_{y_i}}} \left[e^{-\beta \sum_i \Omega_{x_i}} (1-N\varepsilon) + \varepsilon \sum_{y_i \neq x_i} e^{-\beta \sum_i \Omega_{y_i}} \right]\\
&= \frac{1}{\sum_{y_1,\cdots,y_N} e^{-\beta \sum_i \Omega_{y_i}}} \left[e^{-\beta \sum_i \Omega_{x_i}} + \varepsilon \sum_{y_i \neq x_i} e^{-\beta \sum_i \Omega_{y_i}} - e^{-\beta \sum_i \Omega_{x_i}} \right]\\
&= \frac{e^{-\beta \sum_i \Omega_{x_i}}}{\sum_{y_1,\cdots,y_N} e^{-\beta \sum_i \Omega_{y_i}}} + \varepsilon \sum_{y_i \neq x_i} \frac{e^{-\beta \sum_i \Omega_{y_i}} - e^{-\beta \sum_i \Omega_{x_i}}}{\sum_{y_1,\cdots,y_N} e^{-\beta \sum_i \Omega_{y_i}}}
\end{aligned}$$

where the summation $\sum_{y_i \neq x_i}$ involve N terms corresponding to the N state configurations that are different from $\{x_1, \cdots, x_N\}$, each with respect to just one state. In order words it represents a single cell perturbation of the configuration, i.e. Hamming neighbors.

Let

$$P(x_1, \cdots, x_N) = \frac{e^{-\beta \sum_i \Omega_{x_i}}}{\sum_{y_1,\cdots,y_N} e^{-\beta \sum_i \Omega_{y_i}}} \tag{24}$$

It can be shown that is a probability function that sums to 1. It is actually the Boltzman distribution for the energy function given by $\sum_i \Omega_{x_i}$. We can see that the actual probability of the configuration, $\{x_1, \cdots, x_N\}$ is a perturbed version of this Boltzman probability. The amount of perturbation is proportional to the difference in probability with (Hamming) neighbors of the state. Thus,

$$P_\rho(x_1, \cdots, x_N) \approx P(x_1, \cdots, x_N) + \varepsilon \sum_{y_i \neq x_i} P(y_1, \cdots, y_N) - P(x_1, \cdots, x_N) \tag{25}$$

We can compute P_ρ once we have P, the Boltzman probability. We can see that the correction factor will, in general, be small, proportional to ε. It will decrease the probability of the ground state slightly and some of the near ground state probabilities will also tend to decrease. These small changes will break some of the degeneracies in the Boltzman distribution, but the changes will not be large enough to change the order of the low-energy configurations, especially at high temperatures. We present empirical results later on in the paper to validate this observation. However, at very low (near zero) temperatures, the change will be significant since the difference between the probabilities of the ground state and its Hamming neighbors will tend to larger than at high temperatures. In essence, for finite temperature static equilibrium analysis of QCA circuits the effect of tunneling is not significant. This is essentially the conclusion that is also reached by Sturzu *et al.* [30], but using different *ab initio* calculations. Note that the conclusions does not preclude the importance of tunneling energies for dynamic analysis of QCA analysis at finite temperatures.

C. Computing with Semi-Classical Model

The semi-classical probability of state assignment, $P(x_1, \cdots, x_N)$, can be approximated in terms of pairwise kink energies by exploiting the fact that $\Omega_{x_i} \approx \frac{E_i}{1-2\varepsilon}$ as follows.

$$\begin{aligned}
P(x_1, \cdots, x_N) &= \frac{1}{Z} e^{-\beta \sum_i \Omega_{x_i}} && (26)\\
&= \frac{1}{Z} e^{-\beta \sum_i x_i \sqrt{E_i^2 + \gamma^2}} && (27)
\end{aligned}$$

$$\approx \frac{1}{Z'} e^{-\beta \sum_i x_i E_i \frac{1}{1-2\varepsilon}} \quad (28)$$

$$\approx \frac{1}{Z'} e^{-\beta \sum_i x_i \frac{1}{2} \sum_j E_{ij}^{(k)} P_j \frac{1}{1-2\varepsilon}} \quad (29)$$

The magnitude of the polarization of $j-th$ cell, $|P_j|$ is in the order of $1-2\varepsilon$. Thus, the probability can be approximated as function of pairwise energies.

$$P(x_1,\cdots,x_N) = \frac{e^{-0.5\beta \sum_{ij} E_{ij}^{(k)} x_i x_j}}{\sum_{y_1,\cdots,y_N} e^{-0.5\beta \sum_{ij} E_{ij}^{(k)} y_i y_j}} \quad (30)$$

$$= \frac{e^{-\beta \sum_{i,j>i} E_{ij}^{(k)} x_i x_j}}{\sum_{y_1,\cdots,y_N} e^{-\beta \sum_{i,j>i} E_{ij}^{(k)} y_i y_j}} \quad (31)$$

$$= \frac{e^{-\beta \sum_{i,j>i} E(x_i,x_j)}}{\sum_{y_1,\cdots,y_N} e^{-\beta \sum_{i,j>i} E(x_i,x_j)}} \quad (32)$$

The interactions between QCA-cells is captured by the pairwise energy term $E(x_i,x_j)$, which is dependent on the Coulombic interaction between the cells.

It is not necessary to model the interactions of each cell with every other cells as captured in the double summation in the exponent. Due to the $1/r^5$ fall-off of Coulombic interaction between cells, the energy term between the pair of cells that are far away can be ignored. Let $Ne(X)$ represent the set of cells that are within a specified distance, D, i.e. $Ne(X_i) = \{X_j | d(X_i,X_j) \leq D\}$ and d is the Euclidean distance function. The decomposition of the total energy into pairwise interactions, induces a decomposition of the joint probability function.

$$P(x_1,\cdots,x_M) = \frac{1}{Z} \exp\left(-\frac{\sum_{i=1}^{M} \sum_{j=Ne(X_i)} E(x_i,x_j)}{kT}\right) \quad (33)$$

This joint probability can be factored in terms of pairwise functions, which we will term as probability potential functions, $\phi(x_i,x_j) = \exp\left(-\frac{E(x_i,x_j)}{kT}\right)$.

$$P(x_1,\cdots,x_M) = \frac{1}{Z} \prod_{i=1, j=Ne(X_i)}^{i=M} \phi(x_i,x_j) \quad (34)$$

Given this joint probability function, in principle, it is possible to compute the probability of any state configuration or the marginal probability of any particular subset of random variables. However, the computational complexity is exponential if the computations are blind to the factorization possibilities that exist due to the local nature of the Coulombic interactions. Cells that are far away do not interact directly. They only indirectly influence each other through intermediate cell(s) that directly influence each of the two cells. We exploit this to *factorize* the underlying joint probability function into product of joint probability functions over smaller, but overlapping subsets of random variables. The search for the low-energy configurations can then be decomposed into smaller searches over overlapping spaces. The final solution is then constructed by local message passing among these sets.

To understand the factorization process, it is helpful to represent the joint probability function as undirected graphs, with nodes representing the random variables, and links denoting dependencies, quantified by the corresponding probability potential function. The overall probability function is the normalized product of the individual potential functions. This representation is called a Markov graph [24]. Consider a linear arrangement of 9 QCA cells, shown in Fig. 3(a). The Markov graph representation for 1-cell and 2-cell radius of influence are shown in Figs. 3(b) and (c), respectively. Fig. 3(d) shows a 9-cell neighborhood, where there is no approximation about the neighborhood of influence – we have a complete graph.

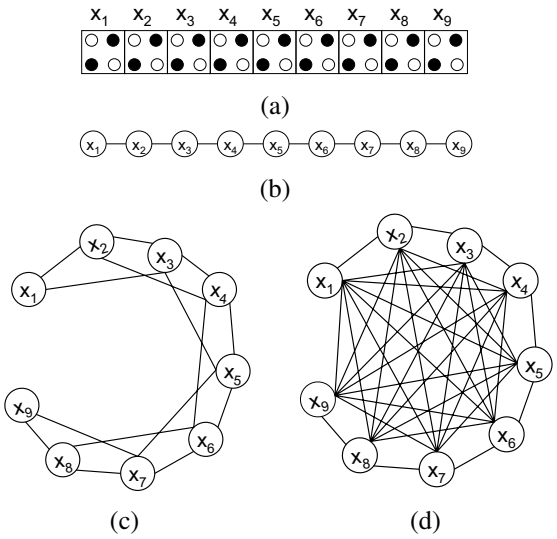

Fig. 3. Markov net dependency model for (a) 9-cell QCA wire considering (b) 1-cell radius of influence (b) 2-cell radius of influence, and (c) all cells. Ignore the link directions.

III. Error Modes of Each Clock Zone

We first consider the probabilistic modeling of state configurations of each clock zone. We will then use these zone based models to construct the spectrum of the complete circuit. To model each zone we have to consider the cells in previous clock zone too, since they act as the driver cells. Given the joint probability specification of the cells in these two zones $P(X_1 = x_1,\cdots,X_n = x_n)$, as captured by the Markov network representation, we explore the computation of the following:

1. Given the polarization of the driver cells in the previous clock zone, $x_1,\cdots,x_r$, what is the *minimum energy* polarization (or most likely state) assignments of all the cells? For this we need to compute $\arg\max_{x_{r+1},\cdots,x_N} P(x_{r+1},\cdots,x_N | x_1,\cdots,x_r)$, or the maximum likelihood state assignments.
2. What are the N-lowest energy configurations for the QCA circuit, for a given driver cell configuration, $x_1,\cdots,x_r$?

Note that these computations are different from the computation of the average case (expected) probabilities, or marginal probabilities, which is commonly considered in most probabilistic analysis [33], [34], [35], [36]. Readers who are familiar with maximum likelihood probabilistic reasoning on graphical models may skip rest of this section.

Instead of approximate schemes, such as those based on "loopy" local message schemes [37], we use an exact inference scheme that also utilizes only *local message passing*, but on

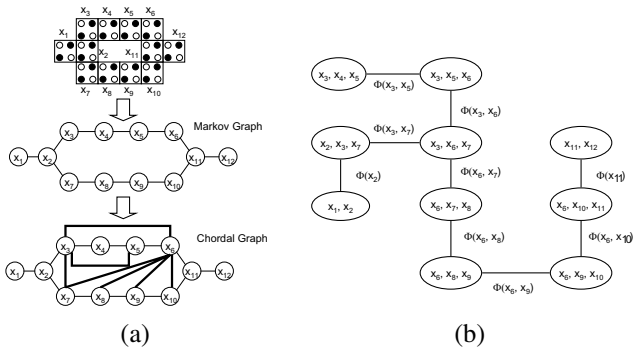

Fig. 4. Graphical dependency structures representing an arrangement of QCA cells. (a) Transformation of a QCA circuit to a Markov network and then to a triangulated graph, capturing only single cell distance interactions. (c) Junction tree of cliques capturing all dependencies.

a tree structured graph to control the computational complexity [24]. The tree-structured graph is made of nodes representing subsets of nodes in the Markov graph and is arrived at via a series of transformations to preserve the represented dependencies. The goal of this transformation is to collect all subsets of random variables that are directly *or indirectly* mutually dependent. Note that the Markov graph links represent the direct dependencies. We need to add the indirect dependencies that are induced in the Markov graph. This, we arrive at by triangulating the Markov graph.

Triangulation is the process of breaking all cycles in the graph to be composition of cycles over just three nodes by adding additional links. There are many possible ways for achieving this. At one extreme, we can add edges between every pair of nodes to arrive at a final graph that is complete, which, of course, will still preserve all dependencies, but will have exponential representational and computational cost. To control the computational demands, the goal is to form a triangulated moral graph with minimum number of additional links. The task of triangulation by adding the minimum number of links is a NP-hard problem. Therefore, in practice one uses various approximate algorithms. For instance, the Bayesian network inference software HUGIN (www.hugin.com), which we use in this work, uses efficient and accurate minimum fill-in heuristics to calculate these additional links. Fig. 4(a) shows a simple arrangement of QCA cells. Its corresponding Markov network, assuming just 1-cell neighborhood of influence, is shown in Fig. 4(b). The triangulated Markov graph is shown in Fig. 4(c).

The triangulation method proceeds as follows. All the nodes of the moral graph are first tagged as unlabeled. An unlabeled node that has the minimum number of mutually unconnected (unlabeled) neighbors is chosen. This node is then labeled with the highest available node number, say i, starting from a number equal to the total number of nodes, N. A set C_i, is then formed consisting of the selected node and its still unlabeled neighbors. Edges are filled in between any two unlinked nodes in this set C_i. Then the maximum available node number i is decremented by 1. This process is repeated until there is no unlabeled nodes. The resultant graph, which we term as the chordal graph, is guaranteed to be triangulated. Note that each C_i is a complete subgraph by construction and the set of these constitutes the cliques of the graph G. The generated sequence of cliques $\mathcal{C}^e = \{C_i\}$'s is termed the *elimination set* of cliques of the graph.

Definition: An *ordering* of the cliques, $[C_1, C_2, \cdots, C_{N_c}]$, is said to possess *running intersection* property if for every $j > 1, \exists i, i < j$ such that $C_j \cap (C_1 \cup C_2 \cdots \cup C_{j-1}) \subseteq C_i$.

This property is essential for inference based on local message passing. The generated order of the cliques in the *elimination set* will possesses this *running intersection* property[24].

It can also be shown [24] that if $C_1, \cdots C_k$ is a sequence of sets with the running intersection property and $C_t \subseteq C_p$ for some $t \neq p$ then the ordered set $C^{'} = \{C_1, \cdots C_{t-1}, C_p, C_{t+1}, \cdots, C_{p-1}, C_{p+1}, C_k\}$ also has running intersection property. Using this property the clique C_t can be eliminated for all $C_t \subseteq C_p, p \neq t$. Hence, the *elimination set* can be reduced to obtain the minimal ordered set of cliques called *clique set*, $\mathcal{C}^t$, representing the triangulated graph completely.

A *junction tree* between these cliques is formed by connecting each C_i to a predecessor clique $C_j, j < i$ in the clique set, $\mathcal{C}^t$, sharing the higher number of nodes with C_i. A junction tree example is shown in Fig. 4(c) for a simple QCA arrangement.

With each clique, C_i, in the junction tree we associate a function, $\phi(c_i)$, also termed as the probability potential function, over the variables in the clique, constructed out of pairwise probability potentials, $\phi(x_i, x_j)$. For each pairwise potential, we find one and only one clique, C_i, that contain the node set $\{x_i, x_j\}$. The potential function for a clique is the product of the conditional probability functions mapped to that clique. Thus,

$$\phi(c_i) = \prod_{\{x_i, x_j\} \in C_i} \phi(x_i, x_j) \tag{35}$$

The joint probability function, which was expressed as product of conditional probabilities, can now be expressed equivalently as the product of these individual clique potentials.

$$p(x_1, \cdots, x_N) = \prod_{c_i \in \mathcal{C}^t} \phi(c_i) \tag{36}$$

The tree structure is useful for local message passing. Given any evidence, messages consist of the updated probabilities of the common variables between two neighboring cliques. Global consistency is automatically maintained by the running intersection property discussed earlier.

A. Maximum Likelihood Propagation

The probabilities are propagated through the junction tree just by local message-passing between the adjacent cliques. The propagation involves two passes through the junction tree. In the first pass, messages are passing from the leaf cliques to an arbitrarily designated root clique. Upon receiving all messages from the leaf cliques, the root clique then initiates the second phase by passing messages to its neighbor. The message passed between two neighboring cliques, C_i and C_j, consists of the marginal over the variables common to them, i.e. their separator set, S_{ij}. The two neighboring cliques have to agree on probabilities over the separator sets. The marginals, $\phi_i(s_{ij})$ and $\phi_j(s_{ij})$, based on the potentials at C_i and C_j, are computed as follows.

$$\phi_i^*(s_{ij}) = \max_{\{C_i - S_{ij}\}} \phi(c_i) \tag{37}$$

$$\phi_j^*(s_{ij}) = \max_{\{C_j - S_{ij}\}} \phi(c_j) \tag{38}$$

If message is being transmitted from C_i to C_j, then the scaling factor $\phi_i^*(s_{ij})$ is transmitted to clique C_j and probability distribution of C_j is rescaled.

$$\phi(c_j) = \frac{\phi_i^*(s_{ij})}{\phi_j^*(s_{ij})}\phi(c_j) \tag{39}$$

New evidence is absorbed into the network by passing such local messages. Because the junction tree has no cycles, messages along each branch can be treated independently of the others and the updating procedure terminates in a time that is linear with respect to the number of cliques.

To find the configuration with this maximum likelihood probability, we start with the root clique; choose its most likely configurations. Then, we move on to its neighbors and choose their most likely configurations, constrained by the configuration of the separator nodes chosen in the root clique. Then the process then continues to the neighbors of the neighbors and so on. The maximum likelihood probability can be simply computed as the product of the probabilities from the individual cliques.

B. N-most Probable Configurations

The search for the N most probable configurations proceeds in an iterative fashion, starting from the most probable configuration [38], [24]. At each iteration, we use the maximum likelihood inference discussed earlier with appropriate constraints. The search for the k-th lowest energy configuration is constrained by the 1-st through $k-1$-th lowest energy configurations found. Let the most likely configuration of variables be denoted by $\mathbf{x}^{(1)} = \{x_1^1, \cdots, x_N^1\}$, with a probability of $P^*(\mathbf{x}^{(1)})$. The second most likely configuration, $\mathbf{x}^{(2)}$ must differ from the most likely configuration in the state of at least one variable. We search for this configuration by performing N maximum propagations with the evidences, F_i, given by

$$F_i = \{X_1 = x_i^1, \cdots, X_{i-1} = x_{i-1}^1, X_i \neq x_i^1\} \tag{40}$$

for $i = 1, \cdots, N$. Let the mostly likely configuration, constrained by the evidence, F_i, be $\mathbf{x}^{(F_i)}$ with probability $P^*(\mathbf{x}^{(F_i)})$. The second most likely configuration will be the most likely configuration with one of these evidences.

$$\mathbf{x}^{(2)} = \arg\max_{\mathbf{x}^{(F_i)}} P^*(\mathbf{x}^{(F_i)}) \tag{41}$$

The third most likely configuration, $\mathbf{x}^{(3)}$, will be from this set of propagations, i.e. one of $\mathbf{x}^{(F_j)}$, or from propagations with evidences that differ from the first and second most likely configurations by at least one state each, F_{ij}.

$$F_{ij} = \{X_1 = x_i^1, \cdots, X_{i-1} = x_{i-1}^1, X_i \neq x_i^1, X_{i+1} = x_{i+1}^1, \cdots, X_j \neq x_j^2\} \tag{42}$$

for $j = 1, \cdots, N-i+1$. Thus, the third most likely configuration is

$$\mathbf{x}^{(3)} = \arg\max \left(\max_{\mathbf{x}^{(F_i)}} P^*(\mathbf{x}^{(F_i)}), \max_{\mathbf{x}^{(F_{ij})}} P^*(\mathbf{x}^{(F_{ij})}) \right) \tag{43}$$

The process continues, until we have N most likely configurations.

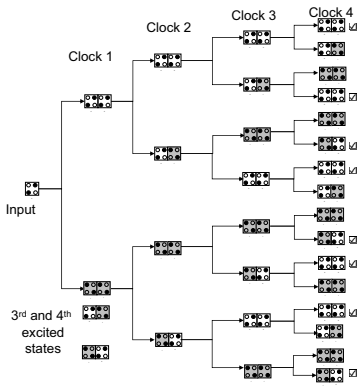

Fig. 5. Energy spectrum tree of a clocked wire segment taking into account the ground state and the first excited state at each zone. Shading is used to denote the two cell states. The configuration that results in the correct output state is marked with a tick mark at the leaf nodes.

IV. Energy Spectrum of Multiple Clocked Zones

In the previous section, we saw how the energy spectrum, along with their cell state configurations, could be computed efficiently for each clock zone. To construct the energy spectrum of the clocked QCA circuits, we use the Markov model based inference mechanism for each clock zone, conditioned on the low-energy states of the previous clock zone. For instance, in the first clock zone, we can compute the ground and the first excited states conditioned on the primary input states. For the second clock zone, we then compute two sets of ground and excited states corresponding to the ground and the excited states of the first clock zone. Similarly, for the third clock zone we have eight sets of configurations. Thus, we construct a tree-like state configuration structure, where each node in the tree corresponds to a state configuration of a clock zone and each level corresponds to a clock zone.

To illustrate, we consider the clocked wire configuration shown earlier in Fig. 1(a). It has 4 clock zones plus the input cell. Each zone has 2 cells. Given the states of the input cell, the two cells in the next clock zone can exist in four possible states, out of which we consider only the ground state and the first excited state. For each of these states for the first clock zone, we consider the ground and first excited states of the second zone. And so on. The resulting tree structure of states is shown in Fig. 5. Note that we can have correct result at the output even with intermediate cell state errors. In practice, we would have to consider all configurations that are close to the ground state as possible branches to explore.

To specify the energy structure, we will extend the mathematical notations we have used so far to include the clock zone. Thus, X_{ij} will denote the i-th cell in the j-th zone. The k-th lowest energy configuration of the cells in the j-clock zone will be denoted by $\mathbf{x}_j^{(k)} = \{x_{1j}^1, \cdots, x_{Nj}^1\}$, with a probability of $P^*(\mathbf{x}_j^{(k)})$. For notational uniformity, we categorize the inputs as being in the first clock zone. For each clock zone, we find the k-lowest energy configuration configurations conditioned on the lowest

energy configurations of the previous clock zone. Thus,

$$\{\mathbf{x}_j^{(1)},\cdots,\mathbf{x}_j^{(km)}\} = \{\arg\max_{\mathbf{x}_j}^{(k)} P^*(\mathbf{x}_j|\mathbf{x}_{j-1}^{(n)}, n=1,\cdots,m\} \quad (44)$$

Note that for each lowest energy configuration, $\mathbf{x}_{j-1}^{(k)}$, of the previous clock zone, we compute k lowest energy configuration of j-th clock zone.

V. Design Metric: Switching Error Likelihood

From a design point of view it is important to study how the probabilities of the low-energy configurations vary with temperature. However, not all of the low-energy configurations result in output errors. To quantify this effect we will assume that in practice a QCA circuit will be adiabatically clocked in an effort to keep the circuit at ground state. Therefore, errors would occur predominantly when the states switch out from the ground state to a near ground state. The near ground states of interest need not be just the first excited state, but could have energies very close to first excited state. The probability of thermal transition (P_{th}) between ground state, with energy E_g and a state with energy E_k is proportional to $\exp(-\beta(E_k - E_g))$. This is equal to the ratio of the probability of excited state to the probability of the ground state.

$$P_{th}(k) = \frac{P_k}{P_g} \quad (45)$$

We consider excited states for which is probability above a fixed probability, say 0.1 or 10% chance of error in state switching. This threshold could be linked to the non-adiabicity of the clocking scheme, however, we do not attempt to explore such linkage here.

To characterize the overall switching stability of a circuit, we will use the ratio of the probability of the error state configurations to the configurations that results in correct output in the ground state and the excited states with $P_{th} > 0.1$.

$$L = \frac{\sum_{P_{th}(i)>0.1,(i)\in\text{error}} \Pr(x^{(i)})}{\sum_{P_{th}(j)>0.1,(j)\in\text{correct}} \Pr(x^{(j)})} \quad (46)$$

We call this ratio the switching error likelihood L and suggest it as design metric. The range of the ratio will vary from 0 to infinity. The lower this value, the better it is in terms of error profiles. Higher values indicate the propensity of switching errors. Note that this is a ratio of two probabilities and hence can be greater than 1.

VI. Results

In this section, we present analyses of basic but critical QCA elements, such as wires, majority gates, and wire crossovers using the graphical probabilistic models presented here. All conclusions are based on the quantum-corrected spectra (Eq. 25), computed after the semi-classical spectra are computed with the Markov models. Although, we do compare this quantum-corrected spectra with the semi-classical one for some QCA circuits to show that the differences are indeed small.

First, we present studies of switching error likelihoods of wires and consider error vs. delay trade-offs. Delay in wire arises from the need to clock the wire transmission. We find that contrary to expectations, placing one cell per clock zone does not result in the most stable solution. Second, we demonstrate the ability of the model to handle an *unbalanced* version of the majority logic gate, for which first order quantum models based on Hartree-Fock approximations have been shown to be inadequate [18] – higher order interactions were necessary to model adequately the dependencies. Third, we present studies with the crossbar architecture, which is an essential component of QCA circuits facilitating the crossing of wires in the 2D plane. Based on studies, we show that some amount of thermal robustness can be achieved either by thickening the design.

It is also worthwhile mentioning that in the experiments, only some of whom we present here, we have validated that our probabilistic model can indeed find all the state configurations, ranked according to energy, by comparing against exhaustive enumeration for small QCA circuits for which such exhaustive exploration is computationally feasible.

A few words about how the thermal studies are presented are in order. The thermal behavior of a QCA circuit is dependent on the kink energy between the QCA cells, which in turn, depends on the physical implementation of the cells; molecular cells have higher kink energy than metal or semiconductor based ones. So instead of reporting the variation directly in terms of the temperature, we consider the kink energy invariant ratio $\frac{kT}{E_k}$, where E_k is the largest kink energy between two QCA cells in the design and k is the Boltzman constant. The dynamics of QCA operation is dependent on this ratio, which will refer to as the normalized temperature (NT).

A. Wires: Thermal, Error, Delay Studies

We first consider the 9-cell QCA wire arrangement shown in Fig. 3(a) but without clocks to validate our computations. QCA wire is a well studied configuration and has been be studied exhaustively [39]. Fig. 6 (a) shows the low energy spectrum computed in four different ways: (i) using semi-classical method with a 2-cell neighborhood model, (ii) using semi-classical method with an all-cells neighborhood model, (iii) after quantum perturbation correction with a 2-cell neighborhood model, and (iv) after quantum perturbation correction with an all-cells neighborhood model. We plot the probabilities of the configuration, but on a logarithmic scale so as to emphasize the differences in the energies between the configurations; the negative log of the probability is proportional to the energy. We can make a number of observations from this plot. First, a 2-cell neighborhood is sufficient; using an all-cells neighborhood does not increase accuracy, but increases the computational cost. Second, semi-classical model seems to be sufficient for ground state and near ground state computations. The quantum-correction factor changes only the high energy states, but that too, slightly (in terms of probabilities). There is some splitting of states, but the associated probabilities are orders of magnitude lower than the ground state. Third, note the clustering of the states to form the first excited cluster, second excited cluster, and so on. The probabilities within each cluster need not be the same (degenerate), but they are very close to each other. Of particular concern is the first excited cluster of states. Fig. 6 (b) shows the 11 lowest energy configurations. Cell states that are different from the ground state are shown as shaded cells. Note that

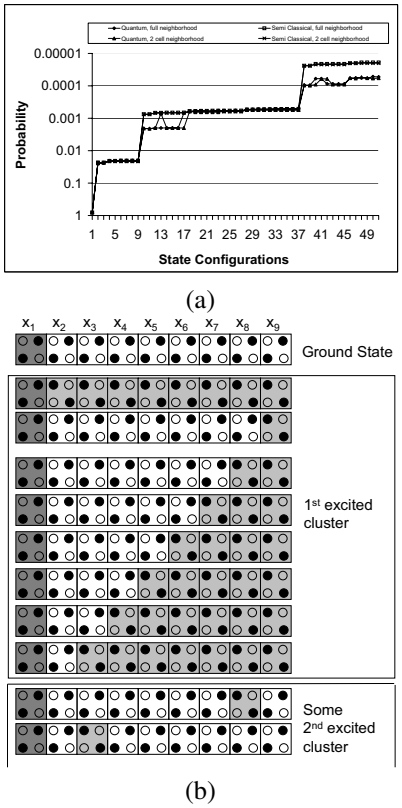

Fig. 6. Study of a 9-cell wire. (a) Low energy spectrum computed using semi-classical and after quantum perturbation correction, with a full 9-cell neighborhood model and a 2-cell neighborhood model. The vertical scale is *logarithmic*, plotted reversely (higher probabilities are down), and denotes the probability. Note that the negative log of the probability is proportional to the energy. (b) Some low energy configurations of a 9 cell QCA wire Cell states that are different from the ground state are shown shaded. Only two of the configurations from the 2^{nd} excited cluster are shown here.

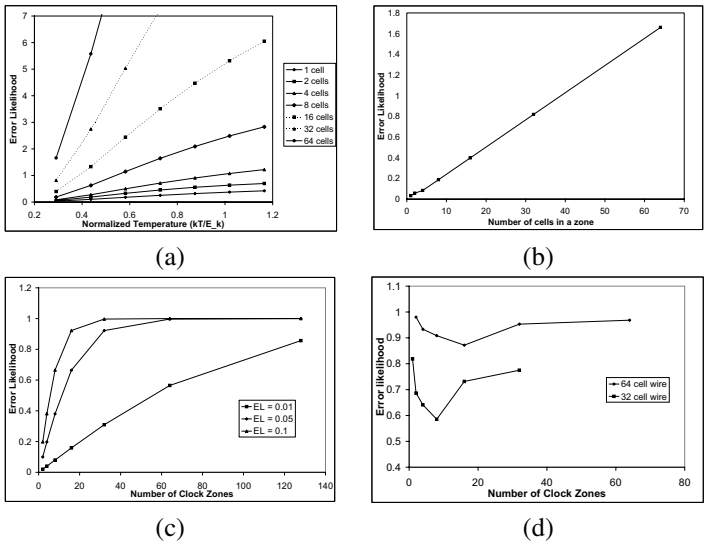

Fig. 7. Switching errors and delay studies of a clocked wire. (a) Variation of error likelihood of one clocked zone in a wire with normalized temperature ($\frac{kT}{E_k}$) for different clock sizes. (b) Variation in error likelihood of one clocked zone with number of cells in that zone. (c) Variation in *overall* error likelihood of a wire with number of clocked zones in that wire for various error likelihoods of *each* clocked zone. (d) Switching error versus delay trade-off for two wire lengths at normalized temperature of 0.291.

the first excited state cluster consists of state configuration with single kinks. The configurations with kinks after the first cell and before the last cell are somewhat higher probabilities than the other first excited state cluster, but very close to them. Configurations with two kinks comprise the next energy band. Note that non-ground states can also result in correct outputs.

Next, we considered clocked wire designs of different lengths ranging from 2 to 128 cells, with different number of clock zones. For each zone, we consider the ground state and the first excited cluster of states. Fig. 7(a) shows the error likelihood variation with temperature of *individual* clock zone with different number of cells. Fig. 7(b) shows the variation of error likelihood with number of cells per zone for a fixed temperature. Note that we are plotting the error likelihood (ratio of error probability to correct probability) which can be greater than one. We notice that

- the variation of error likelihood of *individual clock zones* with normalized temperature ($\frac{kT}{E_k}$) is linear, and
- the variation of error likelihood of an *individual clock zone* with number of cells is also linear.

It would appear that smaller the number of cells per clock zone, the more stable is the wire, but this is not so. For a wire of fixed length as the number of cells per clock zone decrease, the number of clock zones increase. Thus, increasing the number of times errors can occur. For one clock zone, errors can occur during the transition of that clock. For two clock zones, errors can occur during two clock transitions, one in each zone. And so on. The error likelihood of a chain of clock zones can be expressed in terms of the likelihoods of individual zone error likelihoods. Fig. 7(c) shows the variation of *overall* error likelihood of a clock wire with the number of clock zones for different error likelihoods (L) of each clock zone. We see that the *overall* error likelihoods increase with number of clock zones.

We combine the zone error likelihoods at normalized temperature of 0.291 from Figs. 7(a) and (b) with Fig. 7(c) to arrive at a plot of error likelihood of the *overall* clocked wire as a function of the number of clock zones or the overall delay in transmission as shown in Figs. 7(d). We clearly see that neither one clock zone for the entire wire nor the other extreme of one clock zone per cell is the most stable solution. The optimal value lies somewhere it between and appears to be different for different wire sizes.

These kinds of error versus delay studies has implications in design automation of QCA circuits. First, these kinds of studies can be used to build errors macromodels of QCA circuit elements in terms of temperature and clocking structures. For wires, at least, the relationships seems be fairly simple linear one. Second, these kinds of studies will influence the final assignment of clock zones in QCA circuits. So far, current approaches have allocated clock zones purely on timing issues [40]. The analysis presented here will impose additional constraints on the design based on errors. Our study indicates that, contrary to expectations, densely placed (smaller) clocking zones does not guarantee good error performance.

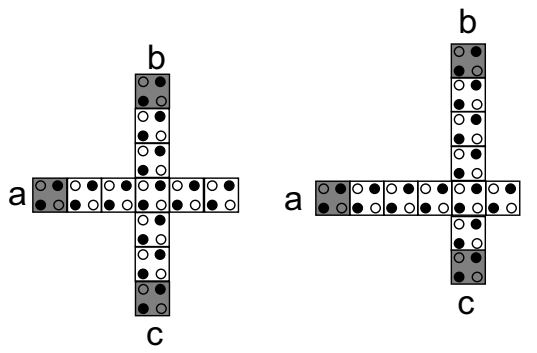

(a)

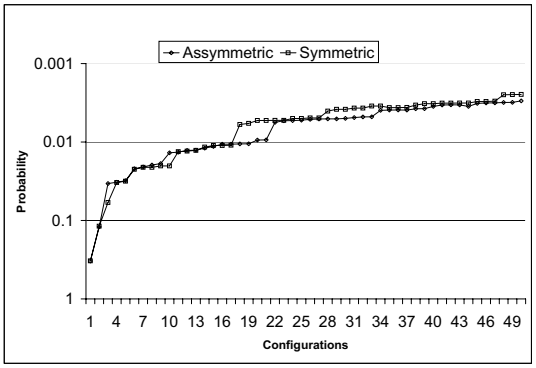

(b)

Fig. 8. (a) Balanced and unbalanced majority gate with same number of cells. (b) State configuration spectrum for balanced and unbalanced majority gate. Note the vertical axis plots the probability on a logarithmic scale, ordered inversely; thus the vertical is proportional to the energy.

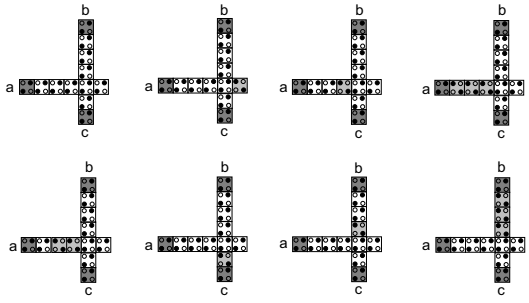

Fig. 9. Low energy configurations of an unbalanced majority gate, with input (0, 0, 0), as computed using maximum likelihood inference with the Markov net model. Cell states that are different from the ground state are shown shaded.

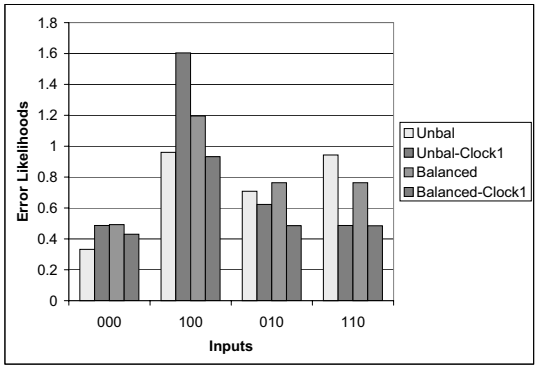

Fig. 10. Variation the error likelihood for different inputs to unbalanced and balanced majority logic gate, with and without clocking. The normalized temperature is 0.582.

B. Majority Logic: Thermal Studies

The basic logic block for QCA designs is the 3-input majority gate. In addition to a balanced majority logic gate (Fig. 8(a)), we also consider a particularly challenging, unbalanced version of the majority gate. The input wire lengths of the unbalanced majority gate are not of the same length. This unbalanced gate was found to be particularly difficult to model. First order Hartree-Fock approximations without accounting for correlations between cells was found to be inadequate [18]. We find that dependency preserving probabilistic models presented here is able to model correctly the unbalanced gate. Fig. 8(b) shows the energy spectrum of the two gates with the same number of cells. We see some minor differences in the spectrum; note that the vertical scale is logarithmic so small differences are emphasized.

Fig. 9 shows the low-energy configurations for the unbalanced majority gate. We found that the ground state configurations for different inputs results in the expected cell configuration of a majority gate. It is interesting to note that the configuration with just the output cell error is the first excited cluster. The next three configurations, constituting the second excited cluster, actually results in correct output, even though there are state errors in the internal cells.

Clocking can introduce some more stability to the operation of a majority logic performance. We considered two clocking zones, one covering the input arms and the other covering the central cell along with the output link. Fig. 10 shows the error likelihood for balanced and unbalanced gates, with and without clocking, and for 4 different inputs. Due to symmetry, the results for the complemented forms of the inputs are the same as that for these 4 inputs. The worst case input is (1, 0, 0). We note that clocking does not lower the errors for all inputs for the unbalanced gate. However, for the balanced majority gate, it does lower the errors. Lusth [41] also noted the asymmetry in the ground state probabilities for a majority logic gate. It has implications in power dissipation with switching of inputs states. As inputs switch, the difference in the corresponding ground state energies has either to be dissipated to the background or acquired from the clock.

C. Crossbar: Clocking and Reliability Studies

Among the most crucial element of QCA circuit designs we have QCA crossbars, i.e. wire that cross each other in the same plane minimally influencing each other. The ability to cross wires in QCA designs has been considered to be one its biggest advantages allowing for planar designs. Consider the arrangement of QCA cells shown in Fig. 11(a), which shows three vertical QCA wires consisting of rotated cells and one horizontal wire. Since the horizontal wire is "cut" by the vertical wire, errors in the horizontal wire are of concern. Figs. 11(b), (c), and (d) shows three switching error modes. Fig. 11(e) shows the excited spectrum of the design at two different temperatures. It plots the logarithm of the probability, which is proportional

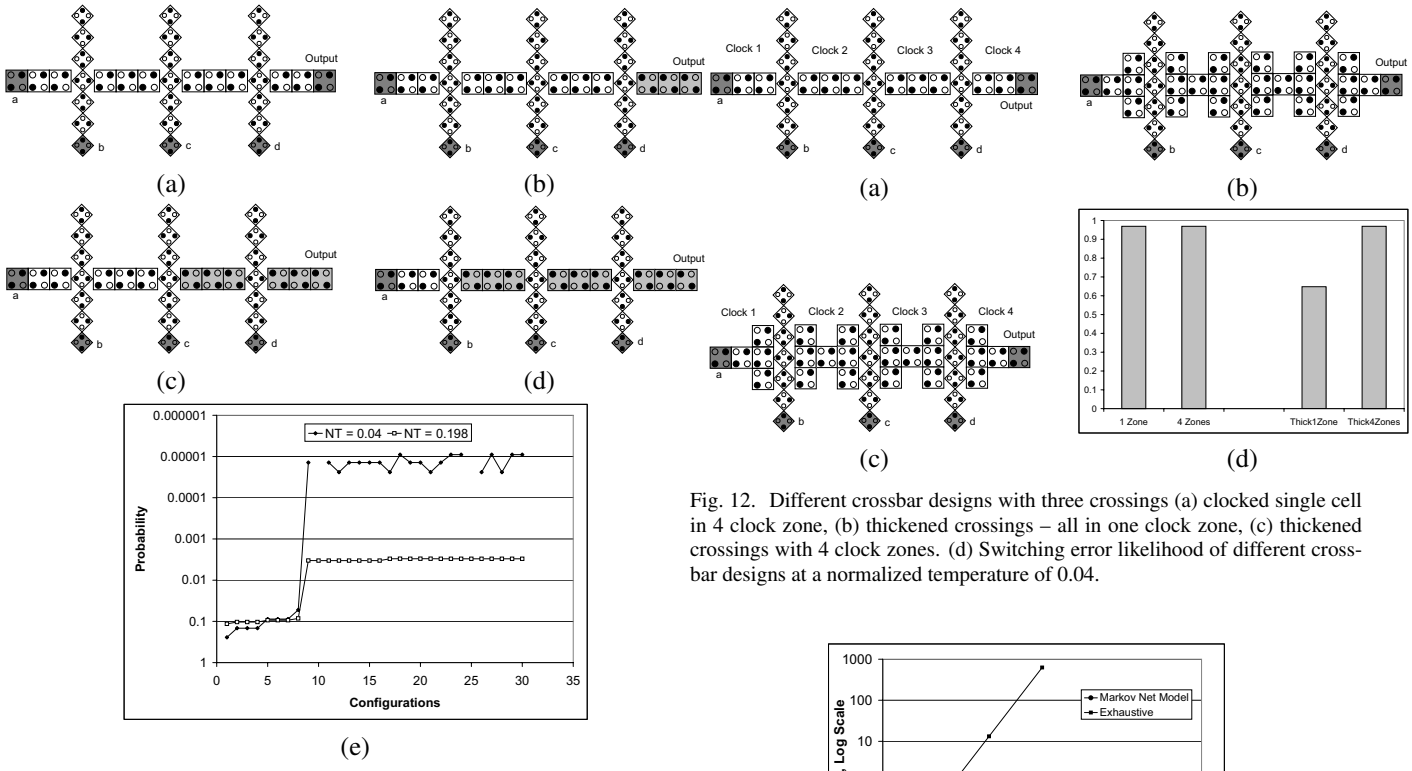

Fig. 11. (a) Consecutive crossbars, all in one clock zone. Errors in the horizontal line are of concern. The switching error modes are shown in (b), (c), and (d). The excited state spectra for the design for two different temperatures are shown in (e). The vertical axis is inversely related to the log of the probability, i.e. it is proportional to the energy.

Fig. 12. Different crossbar designs with three crossings (a) clocked single cell in 4 clock zone, (b) thickened crossings – all in one clock zone, (c) thickened crossings with 4 clock zones. (d) Switching error likelihood of different crossbar designs at a normalized temperature of 0.04.

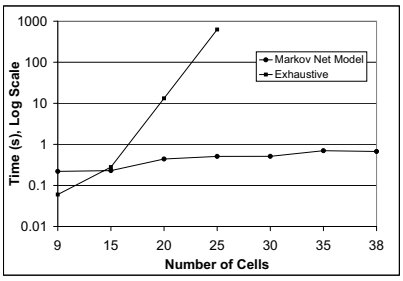

Fig. 13. Comparison of computation times for maximum likelihood inference on Markov net model with exhaustive search on a Pentium III, 800MHz PC with Windows XP. We vary the number of cells in a linear arrangement of QCA cells.

to the energy, of each of the excited state configurations. Note that excited states have very close energy to the ground state, pointing to the inherent instability of the crossbar design. This corroborates the finding of crossbar instability in [42], where 3D designs is suggested to mitigate this effect. We consider mitigation schemes within the constraint of 2D designs.

To harden the design, we use the pattern of the switching error modes in Figs. 11(b), (c), and (d) to partition the circuit into 4 clock zones as shown in Fig. 12(a). In addition, we considered hardening the design at the crossings by thickening them (Fig. 12(b)) and adding clocking zones (Fig. 12(c)). Fig. 12(d) plots the value switching error likelihood for the four crossbar designs at a normalized temperature of 0.04. The switching error modes, not shown here, of all the four designs are the same, except for the difference in the error likelihood values as noted above. We notice that with thickened crossing, the switching error propensity goes down even with one clocking zone. Clocking does not seem to be have much effect in reducing error. The switching error likelihood for thickened and single cell design is similar with addition of clocking zones. However, even with some mitigation, crossbar remains the weakest spot for QCA circuits.

VII. Complexity

The Markov tree based computations are fast. In Fig. 13 we compare the computation times for maximum likelihood inference on Markov net model to search for the 10 lowest energy configurations with exhaustive search for a linear arrangement of QCA cells as the number of cell is varied. We report the total time taken (CPU + I/O) on a Pentium III, 800MHz PC with Windows XP. It includes the time taken to compile the Markov network and the inference times. The vertical axis is a log scale. We see that, as expected, exhaustive search exhibits exponential behavior, unlike that for the Markov net model.

It might appear that Markov network model is able to bypass the combinatorics of computing the ground state of an N cell arrangement, which is known to be NP-hard [43]. However, this is not so. The modeling exploits the factorization possibilities that exist due to spatial separation of cells to arrive at the least complex model. In the worst case, every cell is dependent on every other cell, resulting in a complete graph, with exponential reasoning complexity. In the rest of the section, we derive the order of complexity of reasoning with the Markov model in terms of QCA circuit parameters.

Recall that a compilation process that transforms the Bayesian network structure into a tree of cliques, called the junction tree, precedes the inference process. So, we first look at the complexity of the inference process, which consists of two steps [24]. First, the Markov network is triangulated with the minimum fill-in heuristic based triangulation method whose complexity can be shown to be $O(N+E)$, where N is the num-

ber of nodes and E is the number of links. The cliques of the triangulated graph are extracted during the triangulation process itself. The second step involves the construction of the junction tree which requires one pass through the ordered list of cliques generated during triangulation. The complexity is $O(N_c)$. Thus, *the overall complexity of the compilation process* is $O(E+N+N_c)$.

Next, we consider the complexity of the inference process. Each step of the message passing scheme requires the computation of the marginalized averaged or maximum probabilities, depending on whether we want simple probabilities or maximum likelihood states. The required number of operation for this marginalization at each clique will be proportional to the size of the joint probability function of that clique. From this observation, it can be shown [44] that the inference process is $O(N_c 2^{|C_{max}|})$ time where N_c is the number of cliques and $|C_{max}|$ is the maximum clique size.

Upon adding up the complexity of compilation and the inference process, we infer that the complexity of the overall process is $O(E+N+N_c 2^{|C_{max}|})$. Using the fact that the number of cliques, N_c is less than the number of vertices, N, and the fact that the maximum clique size is greater than the maximum number of parents of any node, i.e. $|C_{max}| > N_p^m$, we have $O(E+N2^{|C_{max}|})$ as the overall complexity. An upper bound on the number of edges, E, can constructed out from the maximum clique size and the maximum number of possible cliques.

$$E \leq N|C_{max}|^2 \tag{47}$$

Using this fact, it is obvious that the exponential term will dominate the complexity, which will be $O(N2^{|C_{max}|})$

A good upper bound on the maximum clique size can arrived at using the bounds on a quantity called the induced width of a graph, which was derived in [44]; we do not describe it here. The original analysis was for directed probabilistic models, we modified the analysis for undirected graphs.

$$|C_{max}| \leq \max_i |Ne(X_i)| + \sum_{Y \in Ne(X_i)} |Ne(Y)| - 1 \tag{48}$$

where $Ne(X)$ refers to the neighbor set of the node X. In the context of QCA circuits, this set will be determined by the neighborhood radius used to model the cell to cell interaction, which would be bounded. Let this radius be r. The total number of neighbors would be bounded by r^2, a constant. Thus, the overall complexity is linear in the number of cells, but exponential with the radius of influence, i.e. $O(N2^{r^4})$. In most cases, a small value of radius $r = 2to5$ cells suffices.

VIII. Conclusions

We proposed a new error analysis formalism that is based on the low energy spectrum that reflects the underlying physics of the operation of QCA cells. Instead of just the ground state cell configuration, as is the current practice, we also compute the low-energy states near it. Starting from a quantum-mechanical formulation of the spectrum, we derived approximations in terms of the semi-classical Gibbs models. We showed that the quantum-mechanical spectra can be expressed, upto a first order approximation, as a perturbation of the semi-classical spectra. We then showed how we can efficiently compute the N-lowest semi-classical energy state configurations by modeling the QCA cell arrangement using a Markov graph-based probabilistic model, which we then transformed into a Markov tree structure defined over subsets of QCA cells. The N-lowest energy configurations were then computed by local message passing; the inference is exact and there are no approximations involved. We showed that the complexity of the inference is polynomial in terms of number of cells, assuming a finite neighborhood of influence for each QCA cell, which is usually the case. We demonstrated the model using QCA circuit structures such as wires, majority gate, and crossover wires. We also demonstrated how the model can be used to study the error configurations of QCA circuits and the variation of the low-energy configuration likelihoods with temperature and conduct error versus delay studies. These issues are important for the design of thermally robust QCA circuits. Current QCA designs take into account just the ground state configuration to map the logic and timing issues to design the clock. The error versus delay studies of the kind presented here places further constraints on high level design.

IX. Acknowledgement

This work is supported in part by the NSF CAREER grant CCF-0639624, NSF Computing infrastructure grant CNS-0551621 and also by the University of South Florida start-up grant.

References

[1] C. S. Lent, P. D. Tougaw, and W. Torod, "Quantum cellular automata: the physics of computing with arrays of quantum dot molecules," in *The Proceedings of the Workshop Physics and Computing*, pp. 5–13, 1994.

[2] M. Cowburn and E. Welland, "Room temperature magnetic quantum cellular automata," *Science*, 2000.

[3] A. Imre, G. Csaba, L. Ji, A. Orlov, G. H. Bernstein, and W. Porod, "Majority logic gate for magnetic quantum-dot cellular automata," *Science*, vol. 311, no. 5758, pp. 205–208, 2006.

[4] W. Hu, K. Sarveswaran, M. Lieberman, and G. H. Bernstein, "High-resolution electron beam lithography and DNA nano-patterning for molecular QCA," *IEEE Transactions on Nanotechnology*, vol. 4, pp. 312–316, May 2005.

[5] A. Fijany, N. Toomarian, K. Modarress, and M. Spotnitz, "Hybrid vlsi/qca architecture for computing FFTs," tech. rep., Jet Propulsion Laboratory, California, Apr. 2003.

[6] M. Niemier and P. M. Kogge, "The "4-diamond circuit" a minimally complex nano-scale computational building block in qca," in *IEEE Computer Society Annual Symposium on VLSI Emerging Trends in VLSI Systems Design*, pp. 3–10, Feb 2004.

[7] J. Timler and C. Lent, "Maxwell's demon and quantum-dot cellular automata," *Journal of Applied Physics*, vol. 94, pp. 1050–1060, July 2003.

[8] D. Marcus, "An investigation of heat dissipation in ultra-dense computer architectures," tech. rep., The MITRE Corporation, 1997.

[9] G. Bernstein, I. Amlani, A. Orlov, C. Lent, and G. Snider, "Observation of switching in a quantum-dot cellular automata cell," *Journal*, vol. 10, pp. 166–173, 1999.

[10] A. Orlov, I. Amlani, G. Toth, C. Lent, G. Bernstein, and G. Snider, "Experimental demonstration of a binary wire for quantum-dot cellular automata," *Applied Physics Letters*, vol. 74, pp. 2875–2877, May 1999.

[11] G. Snider, A. Orlov, I. Amlani, G. Bernstein, C. Lent, J. Merz, and W. Porod, "Quantum-dot cellular automata: Line and majority logic gate," *Japanese Journal of Applied Physics*, vol. 38, pp. 7227–7229, Dec 1999.

[12] I. Amlani, A. Orlov, R. Kummamuru, G. Bernstein, C. Lent, and G. Snider, "Experimental demonstration of a leadless quantum-dot cellular automata cell," *Appllied Physics Letters*, vol. 77, pp. 738–740, July 2000.

[13] A. Orlov, R. Kummamuru, R. Ramasubramaniam, C. Lent, G. Bernstein, and G. Snider, "Clocked quantum-dot cellular automata shift register," *Surface Science*, vol. 532, pp. 1193–1198, 2003.

[14] R. Kummamuru, A. Orlov, R. Ramasubramaniam, C. Lent, G. Bernstein, and G. Snider, "Operation of a quantum-dot cellular automata (qca) shift register and analysis of errors," *IEEE Transactions on Apllied Physics*, vol. 50, pp. 1906–1913, September 2003.

[15] A. Bachtold, P. Hadley, T. Nakanishi, and C. Dekker, "Logic circuits with carbon nanotube transistors," *Science*, vol. 294, pp. 1317–1320, 2001.

[16] D. Srivastava and M. Meyyappan, "Carbon nanotubes," in *Handbook of Nanoscience, Engineering, and Technology* (W. A. Goddard, D. W. Brenner, S. E. Lyshevski, and G. J. Iafrate, eds.), pp. 18–1–18–26, CRC Press, 2003.

[17] M. Niemier, K. M.J., and P. M. Kogge, "A design of and design tools for a novel quantum dot based microprocessor," in *Design Automation Conference*, pp. 227–232, June 2000.

[18] G. Toth, *Correlation and Coherence in Quantum-dot Cellular Automata*. PhD thesis, University of Notre Dame, 2000.

[19] K. Walus, T. Dysart, G. Jullien, and R. Budiman, "QCADesigner: A rapid design and simulation tool for quantum-dot cellular automata," *IEEE Trans. on Nanotechnology*, vol. 3, pp. 26–29, March 2004.

[20] P. Douglas Tougaw and C. S. Lent, "Dynamic behavior of quantum cellular automata," *Journal of Applied Physics*, vol. 80, pp. 4722–4736, Oct 1996.

[21] S. Bhanja and S. Sarkar, "Probabilistic modeling of qca circuits using bayesian networks," *IEEE Transactions on Nanotechnology*, vol. 5, pp. 657–670, Nov. 2006.

[22] M. Macucci, G. Iannaccone, S. Francaviglia, and B. Pellegrini, "Semiclassical simulation of quantum cellular automaton circuits," *International Journal of Circuit Theory and Application*, vol. 29, pp. 37–47, 2001.

[23] J. Pearl, *Probabilistic Reasoning in Intelligent Systems: Network of Plausible Inference*. Morgan Kaufmann Publishers, 1998.

[24] R. G. Cowell, A. P. David, S. L. Lauritzen, and D. J. Spiegelhalter, *Probabilistic Networks and Expert Systems*. New York: Springer-Verlag, 1999.

[25] J. Han, E. Taylor, J. Gao, and J. A. B. Fortes, "Reliability modeling of nano-electronic circuits," *IEEE Conference on Nanotechnology*, 2005.

[26] Y. Qi, J. Gao, and J. A. B. Fortes, "Markov chains and probabilistic computation: A general framework for multiplexed nanoelectronic systems," *IEEE Transactions on Nanotechnology*, vol. 4, pp. 194–205, 2005.

[27] K. Nepal, R. I. Bahar, J. Mundy, W. R. Patterson, and A. Zaslavsky, "Designing logic circuits for probabilistic computation in the presence of noise," in *Design Automation Conference*, pp. 485–490, 2005.

[28] D. Young, *Computational Chemistry: A Practical Guide for Applying Techniques to Real World Problems*. Wiley, 2001.

[29] Y. Wang and M. Lieberman, "Thermodynamic behavior of molecular-scale quantum-dot cellular automata (QCA) wires and logic devices," *IEEE Transactions on Nanotechnology*, vol. 3, pp. 368–376, Sept. 2004.

[30] I. Sturzu, J. Kanuchok, M. Khatun, and P. Tougaw, "Thermal effect in quantum-dot cellular automata," *Physica E: Low-dimensional Systems and Nanostructures*, vol. 27, no. 1-2, pp. 188–197, 2005.

[31] C. Lent and P. Tougaw, "A device architecture for computing with quantum dots," in *Proceeding of the IEEE*, vol. 85-4, pp. 541–557, April 1997.

[32] G. Mahler and V. A. Weberruss, *Quantum Networks: Dynamics of Open Nanostructures*. Springer Verlag, 1998.

[33] S. Bhanja and N. Ranganathan, "Dependency preserving probabilistic modeling of switching activity using bayesian networks," *IEEE/ACM Design Automation Conference*, pp. 209–214, 2001.

[34] S. Bhanja and N. Ranganathan, "Modeling switching activity using cascaded bayesian networks for correlated input streams," *International Conference on Computer Design*, pp. 388–390, 2002.

[35] S. Bhanja and N. Ranganathan, "Switching activity estimation of vlsi circuits using bayesian networks," *IEEE Transactions on VLSI Systems*, pp. 558–567, February 2003.

[36] R. Iris Bahar, J. Mundy, and J. Chen, "A probabilisitic-based design methodology for nanoscale computation," in *International Conference on Computer Aided Design*, pp. 480–486, 2003.

[37] C. Yanover and Y. Weiss, "Finding the M most probable configurations in arbitrary graphical models," in *Advances in Neural Information Processing Systems 16* (S. Thrun, L. Saul, and B. Schölkopf, eds.), Cambridge, MA: MIT Press, 2004.

[38] D. Nilsson, "An efficient algorithm for finding the m most probable configurationsin probabilistic expert systems," *Statistics and Computing*, vol. 8, pp. 159–173, June 1998.

[39] C. S. Lent and P. D. Tougaw, "Lines of interacting quantum-dot cells: a binary wire," *Journal of Applied Physics*, vol. 74, p. 6227, 1993.

[40] M. Niemier and P. M. Kogge, "Exploring and exploiting wire-level pipelining in emerging technologies," in *Proceedings of the 28th annual international symposium on Computer architecture*, pp. 166 – 177, 2001.

[41] J. Lusth, "Balancing qca logic gates under image charge neutralization," in *IEEE Conference on Nanotechnology*, pp. 347–350, 2002.

[42] K. Walus and G. A. Jullien, "Qca co-planar wire-crossing and multi-layer networks," in *iCore Banff Summit*, (Banff, Alberta), June 2004.

[43] T. Cole and J. C. Lusth, "Quantum-dot cellular automata," *Progress in Quantum Electronics*, vol. 25, pp. 165–189, 2001.

[44] R. Dechter, "Topological parameters for time-space tradeoffs," in *Uncertainty in Artificial Intelligence*, pp. 220–227, 1996.